

Effective stability in a moist baroclinic wave

James F. Booth,^{1*} Lorenzo Polvani,² Paul A. O’Gorman³ and Shuguang Wang²

¹Department of Earth and Atmospheric Sciences, City College of New York, NY, USA

²Department of Applied Physics and Applied Mathematics, Columbia University, New York, NY, USA

³Department of Earth, Atmospheric, and Planetary Sciences, Massachusetts Institute of Technology, Cambridge, MA, USA

*Correspondence to:

J. F. Booth, Marshak Science
Building, Room 106, 160
Convent Avenue New York, NY
10031, USA.
E-mail: jbooth@ccny.cuny.edu

Abstract

It has been proposed that the impact of moisture on atmospheric eddy circulations can be approximated using a reduced effective stratification defined in terms of a parameter λ , which quantifies the asymmetry between upward and downward motions. Here λ is analyzed for the midlatitude regime using baroclinic lifecycles computed with the Weather Research and Forecast model. Vertical velocities are compared for integrations with different moisture conditions, and the change in λ is quantified and interpreted. λ is shown to be largely insensitive to grid resolution, and the effective stratification captures the impact of moisture provided initial relative humidity is sufficiently high.

Keywords: atmospheric stratification; baroclinic life cycles; growth rates

Received: 18 November 2013
Revised: 14 July 2014
Accepted: 16 July 2014

1. Introduction

Understanding water’s role in, and its response to, global warming continues to be a fundamental challenge (Stevens and Bony, 2013). In the midlatitudes (as well as the tropics), the response of the atmospheric circulation to greenhouse-gas-induced changes in water vapor remains poorly understood. Ideally, one would like to estimate such a response using theoretical considerations; however, nearly all known scaling laws for midlatitude dynamics rely on dry theory (Holton, 2004). Such laws are likely inappropriate to the moist context, because observations and models show that the presence of moisture greatly affects the circulation within storms (Emanuel *et al.*, 1987), with condensation and deposition the primary mechanisms (Joos and Wernli, 2012).

This effect of moisture on the circulation can be considered either as an external forcing or an altered stratification (Nielsen-Gammon and Keyser, 2000). Regardless, one issue that must be addressed is vertical motion’s asymmetric influence on moisture (and the resulting asymmetry in latent heating): ascending air cools leading to saturation, condensation, and possibly precipitation, whereas descending air warms without normally gaining moisture. This asymmetry is one of the stumbling blocks that prevent the derivation of scaling laws in the presence of moisture, and it is a key factor in determining the intensity distribution of precipitation.

In order to extend dry theories to the moist case, O’Gorman (2011, hereafter OG11) proposed a scaling method focused on the influence of moisture on static stability. OG11 suggests that one might replace dry

stability with an ‘effective’ stability defined by:

$$\left(\frac{\partial\theta}{\partial z}\right)_{\text{eff}} = \frac{\partial\theta}{\partial z} - \lambda \frac{\partial\theta}{\partial z}\Big|_{\theta^*} \quad (1)$$

where $\partial\theta/\partial z$ is the dry stability, λ is the vertical-motion asymmetry parameter, and $\partial\theta/\partial z|_{\theta^*}$ is the vertical gradient of θ at constant saturated moist entropy, assuming hydrostatic balance. The parameter λ is defined as:

$$\lambda \equiv \frac{\overline{\omega'\omega^\dagger}}{\omega'^2} \quad (2)$$

where the prime and overbar represent the eddy and mean with respect to the zonal direction. A truncated vertical velocity, $\omega^\dagger = H(-\omega)\omega$, where $H(\cdot)$ is the Heaviside function, is here introduced to account for the asymmetrical influence of condensation on vertical motion. This definition of λ , therefore, captures the fact that latent heating typically occurs only with upward motion, and λ is closely related to the skewness of the distribution of vertical motions.

To clarify the meaning of λ , OG11 derived an alternative (approximate) definition based on geometric considerations:

$$\lambda_{\text{AREA}} = \frac{1 - a_u}{1 - \overline{\omega}/\overline{\omega_u}} \quad (3)$$

where a_u is the fraction of area covered by the upward motion and $\overline{\omega_u}$ is the spatial average of the upward velocities. This equation was derived assuming a simple piecewise distribution of vertical motion, but it is helpful because it illustrates how λ increases as the area of upward motion contracts.

In OG11, the usefulness of the asymmetry parameter λ was demonstrated by showing how one can incorporate the effective stratification into a variety of dry

scaling laws. This asymmetry parameter has also been utilized in an idealized model to tune the precipitation parameterization (Lambaerts *et al.*, 2012). Given the potential uses of λ , there is a need to further validate its interpretation and to understand moisture's role in setting its value.

The latter remains somewhat tentative. OG11 calculated the value for λ using vertical winds from reanalysis, which may not fully capture moisture's impact on vertical motion. In particular, it is well known that models used in generating reanalyses do not resolve frontal scales (Kanamitsu *et al.*, 2002), and direct observations of vertical velocities are not generally available and thus not assimilated. In fact, such vertical velocities are computed from the model that is used to create the reanalysis. OG11 also calculated λ in climate-model simulations, but climate models have known limitations in both small-scale and moist dynamics (Naud *et al.*, 2010), each of which might affect vertical motion.

In this study, we seek to confirm the mechanisms that contribute to the asymmetry of vertical motion and test the robustness of the numerical value of the asymmetry parameter λ . We accomplish this using integrations of idealized moist baroclinic life cycles with a state-of-the-art weather forecast model. Because such synoptic systems are the primary drivers of vertical motion in winter in the midlatitudes, this experiment is an ideal test bed for the parameter λ . We find here that λ is robustly larger for the moist integrations compared to dry ones, and that the effective stability captures the higher growth rate associated with the presence of moisture. Furthermore, we compute the value of λ at many different resolutions (including a convection-permitting resolution), and show that the vertically averaged value of λ is largely insensitive to the horizontal and vertical grid size.

2. Model and methods

The baroclinic life cycle integrations analysed in this study are described in detail in Ref. Booth *et al.* (2013; hereafter BWP13), so here we only include a few salient facts. They were performed with the Weather Research and Forecast (WRF; Skamarock *et al.*, 2008) model version 3.0.1, configured to solve the non-hydrostatic equations of motion on an f-plane channel, periodic in longitude (x) and with rigid boundaries in latitude (y). Unless otherwise specified, the model domain has 81×181 grid points in the x and y directions, with horizontal grid spacing (DX) equal to 50 km; the vertical domain is discretized with 50 levels. The physics parameterizations used are a cumulus scheme, a microphysics scheme, and a boundary layer scheme; no radiation is present in these integrations. For all further details, the reader should consult BWP13. An additional high-resolution integration is included here (DX = 3.125 km) in which the convection parameterization is turned off.

The WRF model is initialized by prescribing initial temperature and zonal wind profiles, using idealized analytic expressions designed to capture typical wintertime conditions (Polvani and Esler, 2007). To unambiguously document the role of moisture, we focus first on two integrations: an entirely dry one and a moist one. For the moist integration, the initial conditions for wind and temperature are identical to the dry case, and the relative humidity (RH) is again designed to resemble observations (the RH profile is constant in latitude, with RH = 80% at the surface and decreasing with height; see BWP13). Then, we examine two sensitivity experiments from BWP13: (a) the C_{SVP} Experiment, in which the initial RH is fixed and the moisture content is synthetically changed by introducing a coefficient (termed C_{SVP}) in the Clausius–Clapeyron equation:

$$q_{\text{SAT}} = C_{\text{SVP}} * 6.11 * e^{\left(\frac{L_v}{R_v} * \left(\frac{1}{273} - \frac{1}{T}\right)\right)} \quad (4)$$

where L_v is the latent heat of vaporization, R_v , the gas constant of water vapor, and T , temperature in kelvins, and (b) the RH_0 Experiment, in which the initial conditions for the entire vertical profile for RH is multiplicatively shifted using a control parameter RH_0 . By design, RH_0 is also the initial RH at the surface. $C_{\text{SVP}} = 1$ in these integrations.

3. Moist and dry integrations

It is helpful to start by comparing the broad characteristics of the dry and moist baroclinic life cycles. In Figure 1(a), we present the time evolution of the eddy kinetic energy (EKE, defined in BWP13). As is clear from the figure, the moist instability develops faster than its dry counterpart, and the cyclone reaches larger amplitude. Recall that both these integrations have identical temperature and wind initial conditions, so any subsequent difference can be attributed directly to moisture.

Figure 1(b) and (c) shows snapshots of lower tropospheric vertical velocity, ω , during storm development, in the dry and moist cases, respectively. Note how, even in the dry case (Figure 1(b); Table 1), the area of ascent (blue) is smaller than the area of descent (yellow). This is related to the ageostrophic components of the flow in the developing baroclinic wave (Snyder *et al.*, 1991; Rotunno *et al.*, 2000). The asymmetry is amplified in the moist case (Figure 1(c)): see the contraction of the areas of upward motion, especially in the southeast corner of the domain. This scale contraction of the ascending branch has been documented in previous work (Emanuel *et al.*, 1987; Whitaker and Davis, 1994; Fantini, 1995). In addition, we note that the maximum value of ω is larger in the moist case, as the frontal features become sharper.

Next, we calculate λ for the dry and moist lifecycles. We use Equation (2), but we define our eddies by subtracting the area mean, rather than the zonal mean. We do this because it automatically weights to the region of

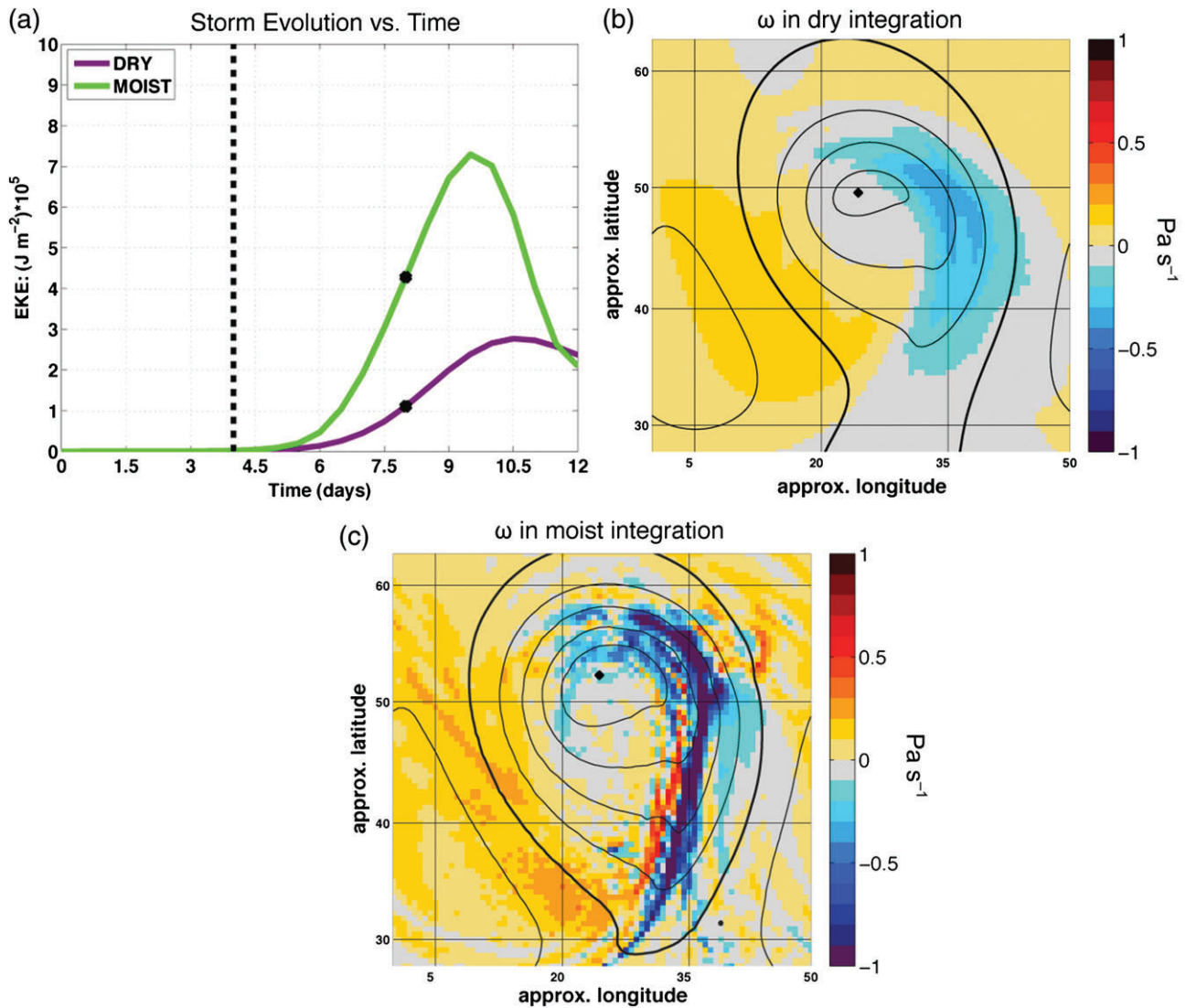


Figure 1. (a) Time evolution of EKE and (b, c) map view of vertical velocity on day 8, at 750 hPa (approximately 2.1 km above the surface) for the dry and moist integrations. In (a), the black dots on the EKE curves mark the times of the snapshots in (b) and (c); dashed line marks start-time for Fig. 2. In (b, c) color shows ω (Pa s^{-1}): red/yellow is downward and gray/blue is upward; black contours show SLP: bold line is 1000 hPa and interval is 5 hPa. The figure does not show the full latitudinal extent of the model.

Table 1. Analytic versus geometric λ .^a

	λ	λ_{AREA}	α_u	$\bar{\omega}$ (Pa s^{-1})	$\bar{\omega}_u$ (Pa s^{-1})
Dry ($C_{\text{SVP}} = 0$)	0.58	0.55	0.45	0.00	-0.03
Moist ($C_{\text{SVP}} = 1$)	0.74	0.64	0.4	-0.004	-0.059

^a λ is the time average from days 4–12.

strong eddy vertical velocities, and λ is then a single number as a function of time and height that captures the updraft/downdraft asymmetry associated with the developing synoptic system.

Figure 2(a) and (b) shows λ for the dry and moist integrations, respectively, with height on the ordinate and time on the abscissa. In both integrations the value of λ is always greater than 0.5, indicating that the upward motions are stronger and cover a smaller area than the downward motions, as already illustrated by the vertical velocity snapshot in Figure 1(b) and (c). Also, comparison of Figure 2(a) and (b) shows that λ is larger in the

moist integration at most heights and times, confirming that moisture enhances the vertical-velocity asymmetry. By day 11 in the moist case (Figure 2(b)), λ is decreasing back towards a value of 0.5. This coincides with the storm reaching its occluded stage and the values of ω becoming smaller as the synoptic wave is dissipated.

Next, we construct a mean value of λ , by averaging in time (from days 4 to 12) and height (from the surface to 10 km). In the dry case, the mean value of λ is 0.58; in the moist run it is 0.74. The latter value is larger than the one found by OG11, whose mean λ in the midlatitudes was 0.55. This difference could be due to multiple factors, which we discuss in Section 6.

To further corroborate our interpretation of λ , we compare the values of λ obtained using the vertical velocities covariance (Equation (2)) and the ascent/descent areas (Equation (3)). For λ_{AREA} , we calculate averages of the variables in Equation (3) over the same vertical levels and days as λ . Table 1

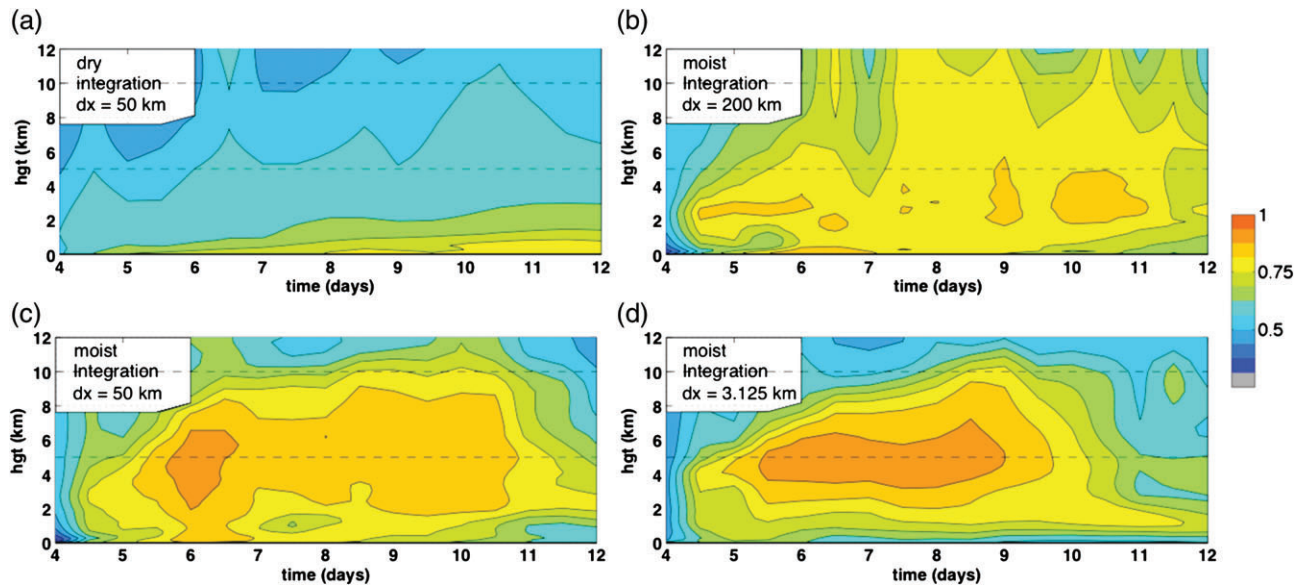


Figure 2. Time versus Height plot of λ calculated using Equation (2); (a) the dry integration at $DX = 50$ km and (b) the moist integration at $DX = 50$ km, (c) at $DX = 200$ km and (d) at $DX = 3.125$ km. For these plots, only the times of cyclone development are shown (Figure 1(a)).

summarizes the results. For both definitions, the dry value is less than the moist value, and for λ_{AREA} this is almost completely determined by the scale contraction of regions of upward motion.

4. The robustness and sensitivity of λ

Since the physical parameterizations relating to moisture, in any model, are often sensitive to the numerical resolution, one might legitimately ask whether the values cited above greatly depend on the grid spacing used. To address this question, we analyze additional integrations with different horizontal grid size (DX) and different numbers of vertical layers (NZ). Recall that the default model configuration is $DX = 50$ km and $NZ = 50$.

First, to test the possible dependence on horizontal grid size, we have computed additional lifecycles using $DX = 3.125$, 25, 100, and 200 km, while fixing $NZ = 50$. The same parameterizations are used in each case, except for the 3.125 km integration, for which we turn off the cumulus parameterization. We note here (but do not show) that the EKE time-series and sea level pressure and synoptic precipitation patterns in the 3.125 km are quite similar to the 50 km integration.

Figure 2(c) and (d) shows $\lambda(z, t)$ for the moist integrations at $DX = 200$ and 3.125 km, respectively. The maximum λ for $DX = 200$ is smaller than in the 50 km case, but the region of large λ reaches higher in the atmosphere. For $DX = 3.125$ km, the maximum value of λ matches that of the 50 km integration (Figure 2(b)) and it is sustained for a longer time. However, the vertical reach of the large λ values is lower in the $DX = 3.125$ cases. Thus, the differences in λ as DX is varied tend to cancel out in a vertical average. The vertical averages are shown in Figure 3(a), where the different colors

indicate different values of DX . It is clear that the vertically averaged values of λ are largely insensitive to DX , and the differences between the moist and dry cases are larger than the differences due to grid spacing.

Perhaps more surprising is the robustness of λ to vertical resolution. We tested such possible sensitivity by carrying out additional moist integrations using $NZ = 25$ and 75, at fixed $DX = 50$ km. The resulting values of λ , for these moist integrations, are shown in Figure 3(b). Again the differences in λ are minuscule as the levels are increased from 25 to 50 to 75.

One might argue that a single integration, at any resolution, might not be sufficient to establish a robust value of λ , owing to the nonlinear and therefore unpredictable nature of baroclinic instability, especially in the presence of moisture (Zhang *et al.*, 2003). To address this, for each of the moist cases shown in Figure 3(a), we computed five-member ensembles by slightly perturbing the initial conditions. The vertical bars surrounding each colored curve in Figure 3(a) show the results: there is very little scatter among the members of each ensemble (except, perhaps, at $DX = 200$ km). Again, λ appears to be robust in our integrations.

Next, we consider the sensitivity of λ to changes in moisture conditions through two different experiments. First, we analyze the C_{SVP} Experiment, in which the moisture content is increased from completely dry ($C_{\text{SVP}} = 0$) to moist ($C_{\text{SVP}} = 1$) in C_{SVP} increments of 0.2 (the completely dry and moist runs are those discussed previously). As discussed in BWP13, C_{SVP} is a control parameter we add to the Clausius–Clapeyron equation to synthetically adjust the moisture content. The RH profile is the same in each of these integrations, so changing C_{SVP} acts to change the amount of moisture that condensates at saturation as well as $\partial\theta/\partial z|_{\theta^*}$ in the effective stability (Equation (1)). Figure 3(c) shows λ

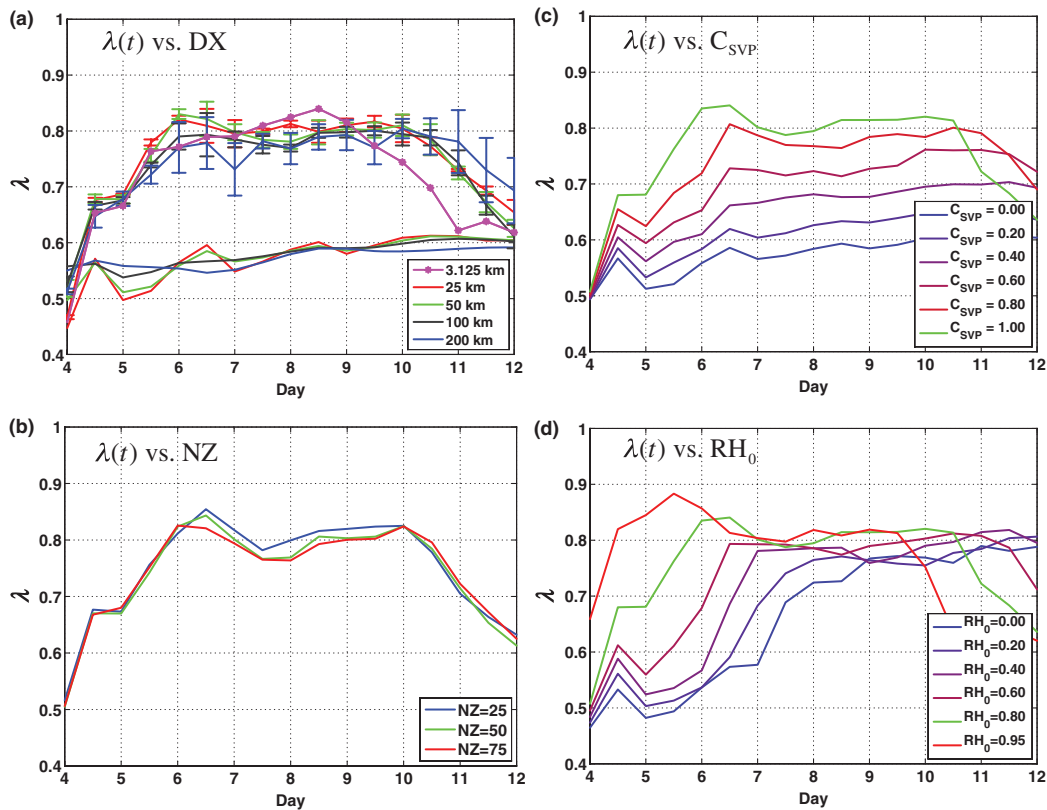


Figure 3. The vertical average of λ from Equation (2), for: (a) different horizontal resolution and (b) different vertical resolution (NZ stands for number of vertical levels), (c) the C_{SVP} integrations and (d) the RH_0 integrations. In (Figure 1(a)), the lower lines with no whiskers are the dry integrations, and the whiskers on the upper lines show bounds based on integrations with small perturbations to initial conditions. The green line in each panel shows the same integration: $DX = 50$ km, $RH_0 = 0.8$, and $C_{SVP} = 1.0$.

for each of the C_{SVP} integrations and there is a clear impact. From day 4.5 through day 12, the dryer runs have weaker λ and thus less asymmetry in their vertical velocity fields.

Finally, we analyze λ for runs with changes in the initial RH. As detailed in BWP13, the initial RH only varies with height, and the vertical profile is defined such that it can be linearly amplified by changing the control parameter RH_0 . Also, if $RH_0 = 0.0$, the initial conditions are dry. However, these integrations occur over a water surface, so surface fluxes add moisture to the $RH_0 = 0.0$ integration as time evolves. Figure 3(d) shows $\lambda(t)$ for the integrations in this experiment. In this case, all the integrations eventually reach the same maximum value for λ . However, in the runs with drier initial conditions λ grows at a much slower pace. In Section 5, we discuss how this impact is manifest in the growth rates.

5. Growth rate estimates

To evaluate the dynamical relevance of the asymmetry parameter λ for the cyclone development, we compare the actual growth rates with the Eady growth rates in the C_{SVP} and RH_0 experiments. For the calculation of the actual growth rates, we use the slope of a line fit to $\log(EKE)$ from day 4.5 through the time each life cycle reaches half of its maximum EKE. We use only the first

half of the growth because the subsequent growth in these waves is nonlinear (Thorncroft *et al.*, 1993). For the Eady growth rate, we use:

$$\sigma_E = 0.31f |\partial U / \partial z| N^{-1} \quad (5)$$

The notation in Equation (5) is standard, with the effective stratification incorporated into N . For all variables in σ_E , we use initial condition data, with the exception of λ , for which we average $\lambda(t)$ over the corresponding time range used in calculating the growth rate from EKE. Furthermore, we use data on the 780-hPa level (as in Hoskins and Valdez, 1990) at the center of the jet (in terms of latitude). We chose this level and latitude because it allows σ_E for the dry integration to exactly match the actual growth rate.

Table 2 summarizes the results for this comparison. For the C_{SVP} experiment, σ_E correctly captures the increase in growth rate as C_{SVP} is increased. As we use initial conditions in calculating σ_E , the only terms that differ per integration are the virtual temperature (which changes by very little) and the terms in the second component of the effective stratification: λ and $\partial\theta/\partial z|_{\theta^*}$. To examine the relative role of λ , which increases (on average) by 0.02 per 0.1 increase in C_{SVP} , we recalculate the Eady growth rates with $\partial\theta/\partial z|_{\theta^*}$ fixed at the value for $C_{SVP} = 1.0$. We find that the increase in λ accounts for about 37% of the increase in σ_E from $C_{SVP} = 0-1$, so that the majority of the increase in growth rate is

Table 2. Actual and estimated growth rates.^a

C_{SVP}	λ	$d\log(EKE)/dt$ (day^{-1})	σ_E (day^{-1})
0	0.56	1.12	1.12
0.2	0.59	1.24	1.20
0.4	0.63	1.3	1.29
0.6	0.67	1.37	1.37
0.8	0.71	1.43	1.46
1	0.77	1.58	1.58
<hr/>			
RH ₀	λ	$d\log(EKE)/dt$ (day^{-1})	σ_E (day^{-1})
0	0.57	1.14	1.41
0.2	0.59	1.17	1.42
0.4	0.64	1.28	1.46
0.6	0.69	1.38	1.50
0.8	0.77	1.58	1.58
0.95	0.84	1.67	1.66

^a λ is the time average during linear growth phase.

due to changes in the moist-adiabatic lapse rate through $\partial\theta/\partial z|_{\theta^*}$. For the RH₀ experiment, λ increases by 0.027 per 10% increase in RH₀. However, σ_E only matches the actual growth rate in the integrations with RH₀ = 80 and 95%.

The different responses of σ_E in the two experiments offer useful information about both the validity and the shortcomings of the effective stratification. On the one hand, changing C_{SVP} can be viewed as varying the initial thermal stratification to be closer or further from moist adiabatic (or changing the temperature in a climate warming experiment with the lapse rate fixed), and in this case the effective stratification accounts for the changes in growth rates. On the other hand, changing the initial RH toward subsaturation led to overestimates of the growth rate. This overestimate is because the derivation of the effective stratification assumes all ascent is saturated, which points to a limitation in the effective static stability as it is currently formulated: it will not properly describe growth in low RH environments. Note, however, that σ_E performs well for both the RH₀ = 80 and 95% cases.

6. Discussion

In summary, using a state-of-the-art weather forecast model, we have shown that moisture increases the asymmetry between updraft and downdraft, as measured by the parameter λ , by roughly 30% for a moist baroclinic lifecycle. When the vertical average of λ is considered, this result is very robust to changes in vertical and horizontal resolution. By confirming this result in an integration run at convection-permitting resolution, we show that the coarse model sufficiently resolves the updrafts and that the cumulus scheme did not disrupt the circulation enough to change λ . However, further work is needed to determine whether this value is more generally applicable to a broader range of conditions (e.g. we have here considered only a single wave type). Also, we note that increasing resolution has a clear impact on the amplitudes of the

strongest vertical motion (not shown), and that resolution affects downstream development (Schemm *et al.*, 2013): thus, coarse-resolution models surely do not capture all impacts of moisture.

The response of λ to changes in moisture content and initial RH help explain what sets the value of λ for our baroclinic wave. For instance, the maximum value of λ varies with changes in C_{SVP} , whereas changes in RH₀ affected the initial value of λ but not its maximum. Both changes in λ and $\partial\theta/\partial z|_{\theta^*}$ contribute to changes in the growth rates in the lifecycles when C_{SVP} is varied. However, the effective static stability overestimates the growth rates when the initial RH is decreased, and further work is needed to generalize the effective static stability to allow for unsaturated ascent.

In our analysis, we found a space and time-averaged value of $\lambda = 0.74$, which is larger than previously calculated for midlatitudes using reanalysis ($\lambda = 0.55$) and in an idealized GCM ($\lambda = 0.6$) by OG11. This discrepancy might partly relate to our use of a weather forecasting model, whose parameterizations are tuned differently from those of climate models. Another possible cause for the higher λ found here is that our baroclinic lifecycles are highly idealized: in the reanalysis and GCM simulations the initial stratification may be somewhat different and the fully developed turbulent dynamics of the atmosphere is at play, with different types of cyclogenesis and other circulation types (e.g. blocks) also present. Also, the reduction in λ in the decaying phase of our moist life cycle suggests that a time and space averaged value for λ will be lower in an atmosphere that has reached a statistical equilibrium for the EKE.

Finally, as already stated in OG11, we emphasize that our ability to incorporate λ into existing theories is greater if λ remains constant with changes in climate. In this study, we find that λ is sensitive to the availability of moisture. However, these results do not necessarily extrapolate to a climate change scenario, because the dry dynamic and thermodynamic initial conditions are held constant in our model. It is possible that changes in the mean state in warmer climates impact the role of moisture on stability. Future work is needed to investigate this.

Acknowledgements

J.F.B. was supported by NASA Postdoctoral Program. P.O.G. was supported by NSF grant AGS-1148594. L.M.P. was supported by NSF grant AGS-XYZ. High-performance computing support from Yellowstone (ark:/85065/d7wd3xhc) was provided by NCAR's Computational and Information Systems Laboratory, sponsored by NSF.

References

- Booth JF, Wang S, Polvani LM. 2013. Midlatitude storms in a moister world: lessons from idealized baroclinic life cycle experiments. *Climate Dynamics* **41**: 787–802.
- Emanuel KA, Fantini M, Thorpe AJ. 1987. Baroclinic instability in an environment of small stability to slantwise moist convection. Part I: Two-dimensional models. *Journal of the Atmospheric Sciences* **44**: 1559–1573.

- Fantini M. 1995. Moist Eady waves in a quasigeostrophic three-dimensional model. *Journal of the Atmospheric Sciences* **52**: 2473–2485.
- Holton JR. 2004. *An Introduction to Dynamic Meteorology*, 4th ed. Academic Press: San Diego, CA, 511 pp.
- Hoskins B, Valdez P. 1990. On the existence of storm-tracks. *Journal of the Atmospheric Sciences* **47**: 1854–1864.
- Joos H, Wernli H. 2012. Influence of microphysical processes on the potential vorticity development in a warm conveyor belt: a case study with the limited-area model COSMO. *Quarterly Journal of the Royal Meteorological Society* **138**: 407–418.
- Kanamitsu M, Ebisuzaki W, Woollen J, Yang S-K, Hnilo JJ, Fiorino M, Potter GL. 2002. NCEP-DOE AMIP-II Reanalysis (R-2). *Bulletin of the American Meteorological Society* **83**: 1631–1643.
- Lambaerts J, Lapeyre G, Zeitlin V. 2012. Moist versus dry baroclinic instability in a simplified two-layer atmospheric model with condensation and latent heat release. *Journal of the Atmospheric Sciences* **69**: 1405–1426.
- Naud CM, Del Genio AD, Bauer M, Kovari W. 2010. Cloud vertical distribution across warm and cold fronts in CloudSat-CALIPSO data and a general circulation model. *Journal of Climate* **23**: 3397–3415.
- Nielson-Gammon JW, Keyser D. 2000. Effective stratification for pseudoadiabatic ascent. *Monthly Weather Review* **128**: 3007–3010.
- O’Gorman PA. 2011. The effective static stability experienced by eddies in a moist atmosphere. *Journal of the Atmospheric Sciences* **68**: 75–90.
- Polvani LM, Esler JG. 2007. Transport and mixing of chemical air masses in idealized baroclinic life cycles. *Journal of Geophysical Research* **112**: D23102, doi: 10.1029/2007JD008555.
- Rotunno R, Muraki D, Snyder JB. 2000. Unstable baroclinic waves beyond quasigeostrophic theory. *Journal of the Atmospheric Sciences* **57**: 3285–3295.
- Schemm S, Wernli H, Papritz L. 2013. Warm conveyor belts in idealized moist baroclinic wave simulations. *Journal of the Atmospheric Sciences* **70**: 627–652.
- Skamarock WC, Klemp JB, Dudhia J, Gill DO, Barker DM, Duda M, Huang X-Y, Wang W, Powers JG. 2008. A description of the advanced research WRF Version 3. <http://www.mmm.ucar.edu/people/skamarock/> (accessed 15 May 2012).
- Snyder C, Skamarock WC, Rotunno R. 1991. A comparison of primitive-equation and semigeostrophic simulations of baroclinic waves. *Journal of the Atmospheric Sciences* **48**: 2179–2194.
- Stevens B, Bony S. 2013. Water in the atmosphere. *Physics Today* **66**: 29–34, doi: 10.1063/PT.3.2009.
- Thorncroft CD, Hoskins BJ, McIntyre ME. 1993. Two paradigms of baroclinic wave life-cycle behaviour. *Quarterly Journal of the Royal Meteorological Society* **119**: 17–55.
- Whitaker JS, Davis CA. 1994. Cyclogenesis in a saturated environment. *Journal of the Atmospheric Sciences* **51**: 889–907.
- Zhang F, Snyder C, Rotunno R. 2003. Effects of moist convection on mesoscale predictability. *Journal of the Atmospheric Sciences* **60**: 1173–1185.